HEFAT2007
5th International Conference on Heat Transfer, Fluid Mechanics and Thermodynamics
Sun City, South Africa
Paper number: EE1

LOW DIMENSIONAL POD-GALERKIN MODELING OF ROLLING MODE IN A FULLY DEVELOPED TURBULENT CHANNEL FLOW

Eljack E. M. * [1,2]
*Author for correspondence
[1] Department of Mechanical Engineering
University of Khartoum
Khartoum, P. O. Box 321
Sudan
E-mail: emeljack@uofk.edu

Kajishima T. [2]
[2] Department of Mechanical Engineering
Osaka University
Yamadaoka, Suita, Osaka, 565-0871
Japan
E-mail: kajisima@mech.eng.osaka-u.ac.jp

ABSTRACT

Low dimensional POD-Galerkin model is developed for a fully developed turbulent channel flow. This model is based on the extraction of the Proper Orthogonal Decomposition (POD) eigenfunctions from a DNS data set of a channel flow at $Re_\tau = 150$. The POD eigenfunctions are optimal in energy sense and ordered with the first eigenfunction represents the most energetic structure. POD analysis shows that, POD mode 1, 2 and 3 capture 63 %, 18% and 8.5% of total kinetic energy, respectively. Stream-wise mode zero (stream-wise rolls) contains about 22% of total energy. A Galerkin projection is then used to drive dynamical systems. To investigate coherent structures near the wall in a low dimensional system, only energetic modes are considered. The coupling of stream-wise and wall-normal velocity components is sustained by the implicit coupling in the POD eigenfunctions. Statistics of the flow which is generated by the model compare fairly well with the corresponding POD reconstruction of DNS data from which POD basis are extracted.

INTRODUCTION

Because of its simple geometry and intensive industrial use, fully developed channel flow figure 1 has been investigated intensively both numerically and experimentally.

The quantitative analysis of low dimensional dynamical systems has been an active area of research in the last 20 years. Most work has concentrated on the analysis of time series data from laboratory experiments or numerical simulations. This paper takes up earlier work begun by Aubry et al. [1], they used a POD basis from previous experimental work and constructed a 10-D model for the wall region of a turbulent boundary layer $0 \leq y^+ \leq 60$. Sanghi and Aubry [2] extended Aubry's study and used 2 stream-wise modes. Berkooz et al. [3], Berkooz et al. [4] used uncoupled velocity components model which permitted the stream-wise and cross-stream components to evolve independently. This recovers the correct long-time behavior of a flow lacking stream-wise variations. Juttijudata et al. [5] applied POD in Squire's coordinate system to obtain basis for low dimensional model. However, in Aubry's model, an inhomogeneous pressure term from outside the theory is needed. To overcome this problem Zhou and Sirovich [6], Webber, Handler and Sirovich [7], Omurtag and Sirovich [8] developed a relatively higher dimensional model by introducing a linear transformation of the full channel eigenfunctions so that they represent the wall eigenfunctions in the wall region. In this paper we combine Aubry's and Sirovich's works by developing a low dimensional model for full channel by using a sub domain in horizontal directions (x , z).

NOMENCLATURE

a_n	POD coefficient
i-D	i dimensions
h	half channel width
k_1, k_3	stream-wise, cross-stream wave numbers
l	cross-stream mode
L_x, L_z	size of space domain in x, z directions
m	stream-wise mode
n	POD mode (wall-normal mode)
Re_τ	Reynolds number = $\frac{u_* h}{\nu}$
R_{ij}	space correlation tensor
S_{ij}	cross-spectra tensor
u_i	i velocity component
u_*	friction velocity
U	mean velocity

Greek letters

α	bifurcation parameter
λ	eigenvalue
ν	viscosity
ν_t	eddy viscosity
ϕ_i	i eigenfunction component
Φ	eigenfunction vector
$\hat{a}$	Fourier transform of the parameter a
$\overline{a}$	time average of a
$< a >$	space average of a
$< \cdot, \cdot' >$	inner product

PROPER ORTHOGONAL DECOMPOSITION

Suppose we have a random velocity field, $u_i(\cdot)$. We seek to find a deterministic vector field $\phi_i(\cdot)$ which has the maximum projection on our random vector field u_i; in a mean square sense. We would like to find a whole new deterministic field represented by $\phi_i(\cdot)$ for which $< |\gamma|^2 >=< |u_i(\cdot)\phi_i^*(\cdot)|^2 >$ is maximized, i.e.,

$$< |\gamma|^2 >= \frac{\langle (\phi_i(\cdot), u_i(\cdot))^2 \rangle}{(\phi_i(\cdot), \phi_i(\cdot))} =$$
$$= \frac{\langle \int_D \int_D u_i(\cdot)\phi_i^*(\cdot)u_j^*(\cdot')\phi_j(\cdot')d(\cdot)d(\cdot') \rangle}{\int_D \phi_i(\cdot)\phi_i^*(\cdot)d(\cdot)}$$

or

$$\int \int_D R_{ij}(\cdot,\cdot')\phi_i^*(\cdot)\phi_j(\cdot')d(\cdot)d(\cdot') = \lambda \int_D \phi_i(\cdot)\phi_i^*(\cdot)d(\cdot) \quad (1)$$

Where $\lambda =< |\gamma^2| >$. So, if $\phi_i(\cdot)$ maximizes (1), it means that if the flow field is "projected" along $\phi_i(\cdot)$, the average energy content (λ) is larger than if the flow field is "projected" along any other mathematical structure, e.g. a Fourier mode. In the space orthogonal to this $\phi_i(\cdot)$ the maximization process can be repeated, and in this way a whole set of orthogonal functions $\phi_i(\cdot)$ can be determined. This method is called proper orthogonal decomposition, or POD. The power of POD lies in the fact that the decomposition of the flow field in the POD eigenfunctions converge optimally fast in L^2-sense. Most importantly, the decomposition is based on the flow field itself: if the flow field is inhomogeneous of finite extent, then Hilbert-Scmidt theory applies and the obtained eigenfunctions (*optimal basis*) are empirical, while if the flow field is homogenous or periodic of infinite extent the eigenfunctions are analytical (sines and cosines).

A necessary condition for $\phi_i(\cdot)$ to maximize expression (1) is that it is a solution of the following Fredholm integral equation of the second type

$$\int_D R_{ij}(\cdot,\cdot')\phi_j(\cdot')d(\cdot') = \lambda\phi_i(\cdot) \quad (2)$$

where, R_{ij} is the space-correlation tensor. This space-correlation tensor is symmetric and positive definite. Therefore, according to the Hilbert-Schmidt theory, equation (2) has a denumerable set of orthogonal solutions $\phi_i(\cdot)$ with corresponding real and positive eigenvalues λ. The eigenvalue with the largest magnitude is the maximum which is achieved in the maximization problem (1). The second largest eigenvalue is the maximum of the maximization problem restricted to the space orthogonal to the first eigenfunction and so on. The eigenfunctions of (2) have some interesting mathematical properties. The eigenfunctions are orthogonal as mentioned, and can be normalized: $\left\langle \phi_i^k(\cdot), \phi_i^l(\cdot) \right\rangle = \delta_{kl}$. The closure of the span of the POD eigenfunctions is equal to the set of all realizable flow fields. Therefore we can use it as a basis for the flow field.

$$u_i(\cdot) = \sum_{n=0}^{\infty} a_n \phi_i^n(\cdot) \quad (3)$$

The random coefficients a_n are determined by projection back onto the velocity field i.e.

$$a_n = \int_D u_i(\cdot)\phi_j^{(n)*}(\cdot)d(\cdot) \quad (4)$$

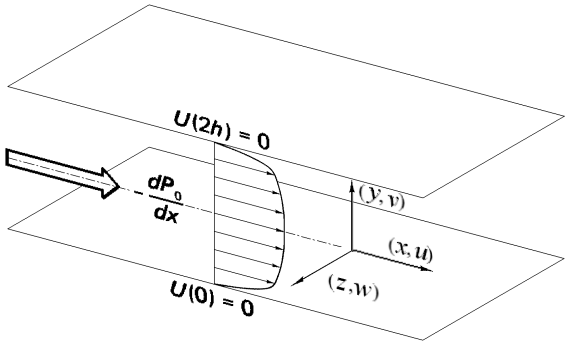

Figure 1: Sketch of the flow geometry

They are uncorrelated and their mean values are the eigenvalues λ

$$\lambda_n =< a_n a_m > \delta_{nm} \quad (5)$$

The eigenvalues are ordered (meaning that the lowest order eigenvalue is bigger than the next, and so on); i.e, $\lambda_1 > \lambda_2 > \lambda_3 \cdots$. Thus the representation is optimal in the sense that the fewest number of terms is required to capture the energy.

APPLICATION OF POD TO CHANNEL FLOW

Figure 1 shows sketch of the flow geometry. Since the flow is periodic in x, homogenous in z and inhomogeneous bounded in y. Fourier transforming equations (2) in x and z directions, space correlation tensor $R_{ij}(x, x', y, y', z, z')$ becomes cross spectra tensor $S_{ij}(y, y'; k_1, k_3)$ and equations (2) can be rewritten as:

$$\int S_{ij\,k_1k_3}(y, y')\phi_{j\,k_1k_3}(y')dy' = \lambda_{k_1k_3}\phi_{i\,k_1k_3}(y) \quad (6)$$

which can be formulated as an eigenvalue problem:

$$A_{ij\,k_1k_3}\phi_{j\,k_1k_3} = \lambda_{k_1k_3}\phi_{i\,k_1k_3} \quad (7)$$

solving these equations numerically for each pair of wave numbers $\left(k_1 = \frac{2\pi m}{L_x}, k_3 = \frac{2\pi l}{L_z}\right)$ yields POD basis ϕ_1, ϕ_2 and ϕ_3 and eigenspectra λ. This process was done for three different integration domains: $D1$ $(256 \times 130 \times 256)$ which covers all the flow field, $D2$ $(256 \times 130 \times 32)$ which covers all the flow field in stream-wise and wall-normal directions and 32 data points in cross-stream direction picked at the middle of the channel, and $D3$ $(32 \times 130 \times 32)$. Figure 2 shows an approximate boundary sketch of these integration domains.

Eigenfunctions:

The eigenfunctions are functions of y in addition to (k_1, k_3). Thus they contain the information about how the energy is distributed in the wall-normal direction for the various modes. Moreover, they contain implicitly the coupling information of various velocity component.

Kinetic Energy:

The total kinetic energy ξ_t is the sum over all POD modes, stream-wise modes and cross-stream modes.

$$\xi_t = \sum_n \sum_m \sum_l \lambda_{ml}^{(n)} \tag{8}$$

from which, energy percentage as a function of stream-wise mode index m, wall-normal mode index n and cross-stream mode index l is given by:

$$\xi^{(n)} = \frac{\sum_m \sum_l \lambda_{ml}^{(n)}}{\sum_n \sum_m \sum_l \lambda_{ml}^{(n)}}; \quad \xi_l = \frac{\sum_n \sum_m \lambda_{ml}^{(n)}}{\sum_n \sum_m \sum_l \lambda_{ml}^{(n)}}$$

$$\xi_m = \frac{\sum_n \sum_l \lambda_{ml}^{(n)}}{\sum_n \sum_m \sum_l \lambda_{ml}^{(n)}}; \quad \xi_m^{(1)} = \frac{\sum_l \lambda_{ml}^{(1)}}{\sum_n \sum_m \sum_l \lambda_{ml}^{(n)}}$$

Figure 3:a shows the energy distribution among the first 13 POD modes for $D1$, $D2$, and $D3$. About 90% of the energy is recovered from the first three POD modes in the three cases. Figures 3:b, c, and d show the energy distribution among the first 16 cross-stream modes, first 16 stream-wise modes, and first 16 stream-wise modes for POD mode 1 only. Kinetic energy distribution in stream-wise and cross-stream directions changes drastically when $D2$ or $D3$ is used rather than $D1$. This change in kinetic energy is due to the fact that a single eddy pair is contained in $D2$ and $D3$, and about 9 eddy pairs are contained in $D1$ in cross-stream direction. When more than one eddy pair is included in the integration domain, POD distribute the energy over the number of eddy pairs for each mode.

In the present study, the POD eigenspectra has an off origin peak corresponding to cross-stream wavelength 144 wall units; this corresponds to the wavelength for recurrence of eddy pairs. So, this justifies that D1 contains about 9 eddy pairs and consequently D2 and D3 contain a single eddy pair. There is no mathematical or physical justification for a recurrence period for coherent structure in the stream-wise direction.

Figure 4 shows the total kinetic energy sum as a function of number of modes for the three integration domains $D1$, $D2$, and $D3$. For $D3$ 150 modes are sufficient to recover more than 90% of total kinetic energy (POD mode 1, 2, and 3, stream-wise mode $0, \pm1$, and ±2, cross-stream mode $0, \pm1, \pm2, \pm3, \pm4$, and ±5). Energy recovery is highly dependent on the size of integration domain, to illustrate this, the zoom-in box in figure 4 shows total energy sum for modes index 1 to 150.

Reconstruction of the instantaneous velocity field

To understand how the POD represents the original velocity signal, the instantaneous velocity field was reconstructed. The doubly Fourier transformed random velocity component, $\hat{\hat{u}}_{ik_1k_3}(y,t)$, can be reconstructed from the eigenfunctions as follow:

$$\hat{\hat{u}}_{ik_1k_3}(y,t) = \sum_{n=1}^{\infty} a_{k_1k_3}^{(n)}(t)\phi_{ik_1k_3}^{(n)}(y) \tag{9}$$

$$S_{ij\,k_1k_3}(y,y') = \sum_{n=1}^{\infty} \lambda_{k_1k_3}^{(n)} \phi_{ik_1k_3}^{(n)}(y)\phi_{jk_1k_3}^{(n)*}(y') \tag{10}$$

$$< u_i u_j >= \sum_n \sum_m \sum_l \lambda_{ml}^{(n)} \phi_{iml}^{(n)}(y)\phi_{jml}^{(n)*}(y) \tag{11}$$

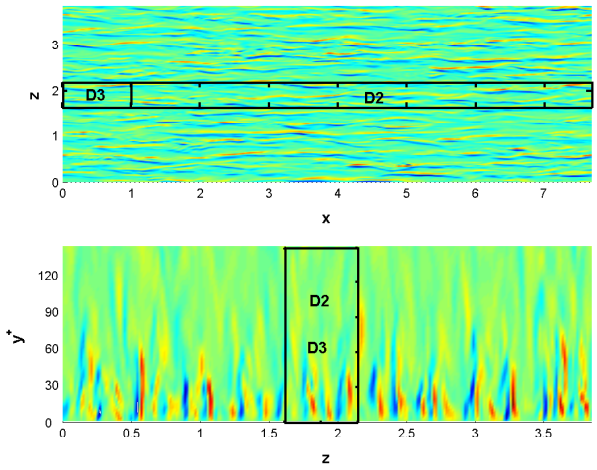

Figure 2: Surface plot of stream-wise vorticity in $x-z$ and y^+-z planes. An approximate boundary sketch of 2 integration domains $D2$ and $D3$ are shown.

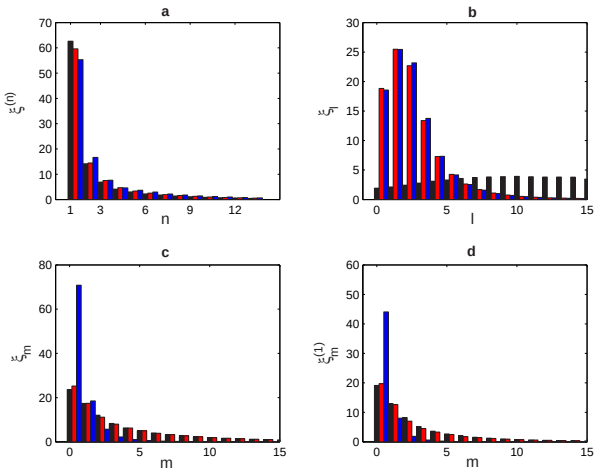

Figure 3: Kinetic energy distribution among cross-stream modes, POD modes, and stream-wise modes for integration domains $D1$ ■, $D2$ ■, and $D3$ ■.

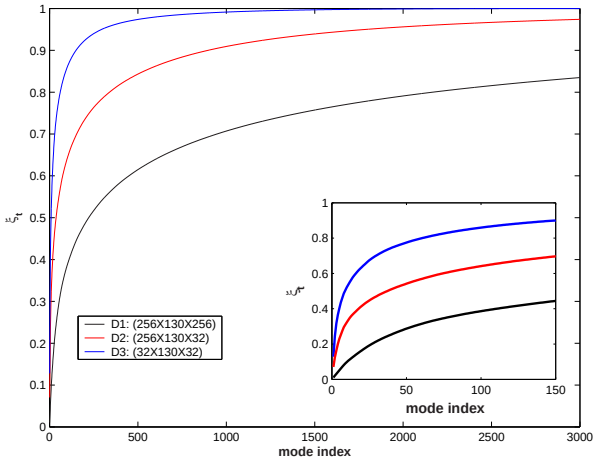

Figure 4: Cumulative energy sum, mode index (m,n,l).

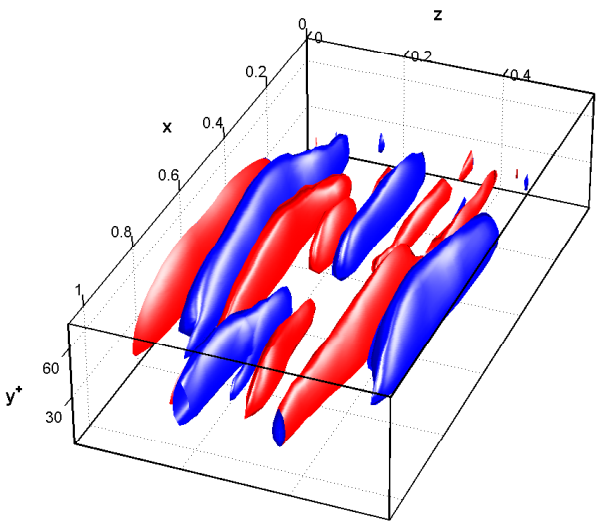

Figure 5: Isosurface of stream-wise vorticity reconstructed using modes $(0, 1, l)$. Red $+ve$, blue $-ve$

FORMULATION OF THE MODEL

momentum equations:

$$\frac{\partial \tilde{u}_i}{\partial t} + \tilde{u}_j \frac{\partial \tilde{u}_i}{\partial x_j} = -\frac{1}{\rho}\frac{\partial \tilde{p}}{\partial x_i} + \nu \frac{\partial^2 \tilde{u}_i}{\partial x_j^2}$$

$\tilde{u_i} = U_i(y,t) + u_i(x,y,z,t)$
define space average as:

$$F_i(y,t) =< \tilde{f}_i >= \frac{1}{L_x L_z}\int_0^{L_x}\int_0^{L_z} \tilde{f}_i(x,y,z,t)dzdx$$

mean momentum equation:

$$\frac{\partial U}{\partial y} = \frac{u_*^2}{\nu}(1-\frac{y}{h}) + \frac{1}{\nu} < uv >$$

$$U(y,t) = \frac{u_*^2}{\nu}(y - \frac{y^2}{2h}) + \frac{1}{\nu}\int < uv > dy$$

fluctuation equations:

$$\frac{\partial u_i}{\partial t} + U_j\frac{\partial u_i}{\partial x_j} + u_j\frac{\partial U_i}{\partial x_j} + \frac{\partial u_i u_j}{\partial x_j} - \frac{\partial < u_i u_j >}{\partial x_j} = \\ = -\frac{1}{\rho}\frac{\partial p}{\partial x_i} + \nu\frac{\partial^2 u_i}{\partial x_j^2}$$

substitute from mean momentum equation and rearrange the terms:

$$\frac{\partial u_i}{\partial t} + \frac{1}{\rho}\frac{\partial p}{\partial x_i} = l(u_i) + q(u_i,u_j) + c(u_i, < uv >) \quad (12)$$

where, l is a linear term, q is a quadratic term and c is a cubic term given by:

$$l(u_i) \equiv \nu\frac{\partial^2 u_i}{\partial x_j^2} - \left[\frac{u_*^2}{\nu}(y - \frac{y^2}{2h})\right]\frac{\partial u_i}{\partial x} - \delta_{i1}\left[\frac{u_*^2}{\nu}(1-\frac{y}{h})\right]v$$

$$q(u_i,u_j) \equiv -\frac{\partial u_i u_j}{\partial x_j} + < \frac{\partial u_i u_j}{\partial x_j} >$$

$$c(u_i, < uv >) \equiv -\left[\frac{1}{\nu}\int < uv > dy\right]\frac{\partial u_i}{\partial x} - \delta_{i1}\left[\frac{1}{\nu} < uv >\right]v$$

u_i expansion from POD basis ϕ_i:

$$u_i = \frac{1}{\sqrt{L_x L_z}}\sum_{n=1}^{\infty}\sum_{k_1,k_3=-\infty}^{\infty} a^{(n)}_{k_1k_3} e^{(ik_1x + ik_3z)}\phi^{(n)}_{ik_1k_3} \quad (13)$$

$$\hat{u}_{ik_1k_3}(y,t) = \sum_{m=1}^{\infty} a^{(m)}_{k_1k_3}(t)\phi^{(m)}_{ik_1k_3}(y) \quad (14)$$

Reynolds stress can be formulated as follow:

$$< uv >= \frac{1}{L_x L_z}\sum_{r,q,k_1,k_3} a^{(r)}_{k_1k_3} a^{(q)*}_{k_1k_3}\phi1^{(r)}_{k_1k_3}\phi2^{(q)*}_{k_1k_3} \quad (15)$$

Fourier transforming equations (12) in the horizontal directions yields a new equations (12*), substitute (14) for $\hat{u}_{ik_1k_3}$ and (15) for $< uv >$ into (12*), applying Galerkin projection and rearranging the terms yields a general dynamical equations as follow: (hereafter, we will use modes index (m,l) rather than wave-numbers ($k_1 = \frac{2\pi m}{L_x}$, $k_3 = \frac{2\pi l}{L_z}$))

$$\frac{d}{dt}a^{(n)}_{ml} = \sum_p L^{np}_{ml}a^{(p)}_{ml} + \sum_{r,q,m',l'} Q^{nrq}_{mlm'l'}a^{(r)}_{m'l'}a^{(q)}_{m-m'l-l'} + \\ + \sum_{r,q,s,m',l'} C^{nrqs}_{mlm'l'}a^{(s)}_{ml}a^{(r)}_{m'l'}a^{(q)*}_{m'l'}$$

$$L^{np}_{ml} = \frac{(1+\alpha\nu_t)}{Re_\tau}\{-4\pi^2(\frac{m^2}{L_x^2} + \frac{l^2}{L_z^2})\delta_{pn} + \\ + \int_{-1}^{1}(\frac{d^2}{dy^2}\phi^{(p)}_{i_{ml}})\phi^{(n)*}_{i_{ml}}dy\} - \\ -\frac{u_*^2}{\nu}(\frac{2\pi i m}{L_x})\int_{-1}^{1}(y - \frac{y^2}{2h})\phi^{(p)}_{i_{ml}}\phi^{(n)*}_{i_{ml}}dy - \\ -\frac{u_*^2}{\nu}\int_{-1}^{1}(1-\frac{y}{h})\phi2^{(p)}_{ml}\phi^{(n)*}_{i_{ml}}\delta_{i1}dy$$

$$Q^{nrq}_{mlm'l'} = -\frac{(1-\delta_{\mathbf{k}0})}{\sqrt{L_x L_z}}\int_{-1}^{1}[2\pi i\frac{(m-m')}{L_x}\phi1^{(r)}_{m'l'}\phi_{i^{(q)}_{m-m'l-l'}} + \\ +\phi2^{(r)}_{m'l'}\frac{d}{dy}\phi^{(q)}_{i_{m-m'l-l'}} + 2\pi i\frac{(l-l')}{L_z}\phi3^{(r)}_{m'l'}\phi^{(q)}_{i_{m-m'l-l'}}]\phi^{(n)*}_{i_{ml}}dy$$

$$C^{nrqs}_{mlm'l'} = -\frac{Re_\tau}{L_x L_z}\int_{-1}^{1}\phi2^{(s)}_{ml}\phi1^{(n)*}_{ml}\left[\phi1^{(r)}_{m'l'}\phi2^{(q)*}_{m'l'}\right]dy - \\ -\frac{2\pi i m}{L_x}\frac{Re_\tau}{L_x L_z}\int_{-1}^{1}\phi^{(s)}_{i_{ml}}\phi^{(n)*}_{i_{ml}}\left[\int\phi1^{(r)}_{m'l'}\phi2^{(q)*}_{m'l'}dy\right]dy$$

Modeling of higher modes:

In Low dimensional models a few modes (lower modes) are resolved and higher modes are ignored. The higher modes represent dissipation. Hence, ignoring them makes the system behave more energetically. To model a real flow, higher modes should be accounted for by means of an eddy viscosity model which assumes that the higher order stress is proportional to the lower order rate of strain and proportionality constant is the eddy viscosity ν_t.

Symmetries of POD basis and modal coefficients:

POD eigenfunctions and coefficients have the following symmetries:

- $a_{ml}^{(n)} = a_{-m-l}^{(n)*}$
- $\Phi_{-ml}^{(n)} = (\phi_{1}{}_{ml}^{(n)*}, \phi_{2}{}_{ml}^{(n)*}, -\phi_{3}{}_{ml}^{(n)*})$
- $\Phi_{m-l}^{(n)} = (\phi_{1}{}_{ml}^{(n)}, \phi_{2}{}_{ml}^{(n)}, -\phi_{3}{}_{ml}^{(n)})$
- $\Phi_{-m-l}^{(n)} = (\phi_{1}{}_{ml}^{(n)*}, \phi_{2}{}_{ml}^{(n)*}, \phi_{3}{}_{ml}^{(n)*})$

which implies that it is only necessary to solve for positive mode index, since the negative mode index (wave number) can be obtained using the above symmetries. For example if we want to solve 11 modes model like $\{(m = 0), (l = 0, \pm1, \pm2, \pm3, \pm4, \pm5)$, and $(n = 1)\}$, practically only 6 equations will be solved. In this case, we discount $a_{00}^{(1)}$ corresponding to mean flow. Furthermore, when computing cross-spectra tensor and solving POD eigenvalue problem for each pair of wave numbers (k_1, k_3), solving for positive wave number only is sufficient to produce eigenfunctions for the model.

MODEL BEHAVIOR

Numerical experiments were carried out with low dimensional model using the following set of modes; stream-wise: $(m = 0)$, cross-stream: $(l = 0, \pm1, \pm2, \pm3, \pm4, \pm5)$, wall-normal: $(n = 1)$, constructing a 5-D model based on integration domain 2 ($D2$). These modes contains approximately 22% of total kinetic energy, the remaining higher modes are accounted for using the eddy viscosity model ($\nu_t = 2.4$). This set of modes were selected based on figure 3:$D2$. A fourth-order Runge-Kutta method was used to solve the system of equations with initial time step 0.02 (the code reduces the time step systematically if it does not guarantee convergence). Different values of the bifurcation parameter α were used to examine model behavior when we overestimate and underestimate the dissipation. It is well known that, in the theory of dynamical systems, the so-called butterfly effect denotes sensitive dependence of nonlinear differential equations on initial conditions. However, initial conditions must be supplied to the dynamical systems model. In Aubry's work, initial conditions were selected to represent the various invariant subspaces in the system of ODE's. In the present study we reconstructed POD coefficients from DNS data using equation (4), then we used a set of values at a single snapshot to be initial conditions for our model.

Figure 6 shows samples time histories of the obtained solutions for $\alpha = 1.67, 1.45, 1.17$, and 0.83. To make sure transient solutions are not adopted, the first $30,000$ data points of the solutions were removed from time histories. Projections of the solutions into the $(\Re(a_{02}), \Im(a_{02}))$ and $(\Re(a_{02}), \Re(a_{04}))$ Phase-planes are shown in figures 7 and 8, which show periodic motion ($\alpha = 1.67$) and quasi-periodic motion ($\alpha = 1.45, 1.17$ and 0.83). Figure 9 shows comparison of POD eigenvalues and the corresponding eigenvalues calculated from modal coefficients using: $\left(\lambda_{0l}^{(1)} = \overline{a_{0l}^{(1)} a_{0l}^{(1)*}}\right)$. When POD and model eigenvalues are not comparable to each other solutions were rejected. Figure 10 shows how model u_{rms} compares to the corresponding POD u_{rms}.

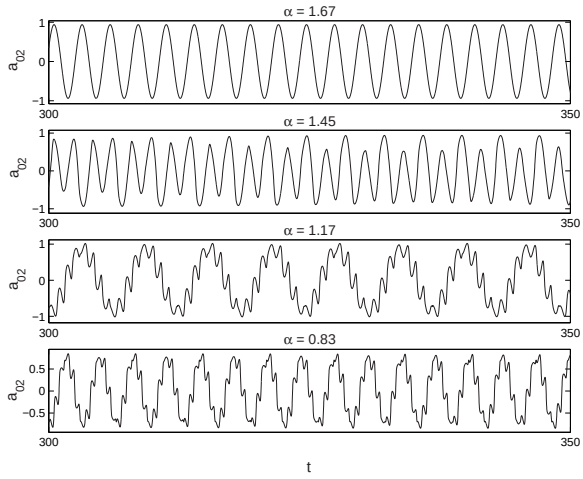

Figure 6: Time histories of real part of a_{02} for different values of α.

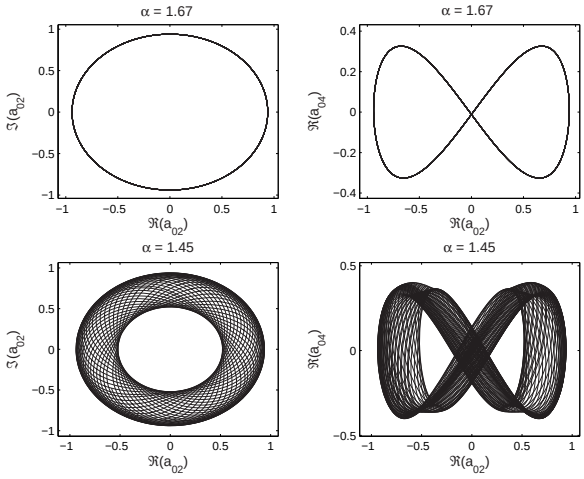

Figure 7: Projections of the solutions into the $(\Re(a_{02}), \Im(a_{02}))$ and $(\Re(a_{02}), \Re(a_{04}))$ Phase-planes.

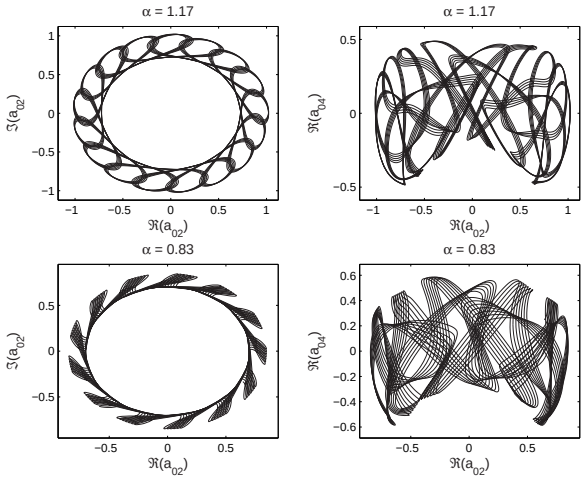

Figure 8: Projections of the solutions into the $(\Re(a_{02}), \Im(a_{02}))$ and $(\Re(a_{02}), \Re(a_{04}))$ Phase-planes.

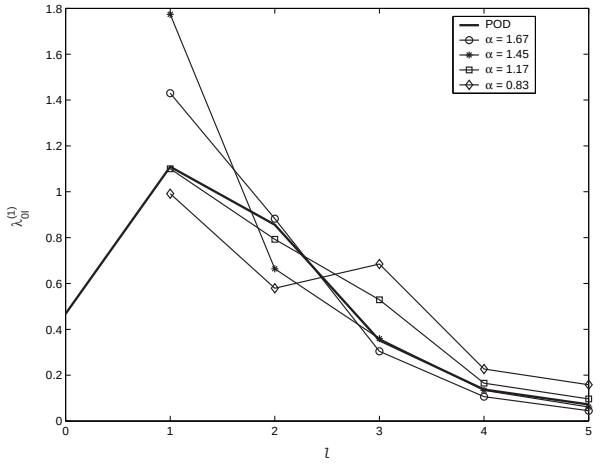

Figure 9: POD eigenvalues $\lambda_{0l}^{(1)}$ modes $(0, 1, 0:5)$, compared with $\overline{a_{0l}a_{0l}^*}$ plot for $\alpha = 1.67, 1.45, 1.17, 0.83$.

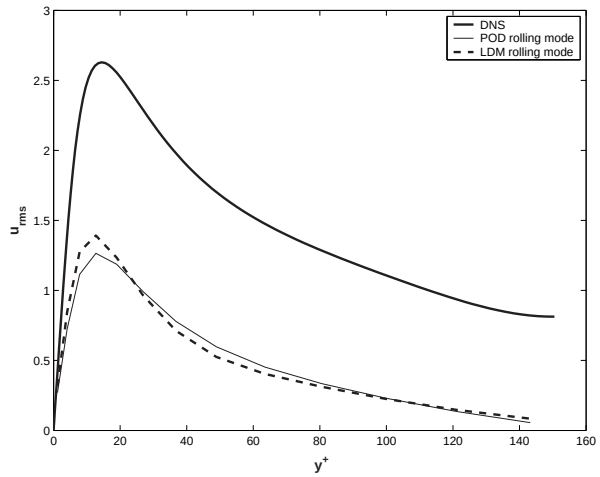

Figure 10: plot of DNS data u_{rms}, POD reconstruction of u_{rms} using modes (0, 1, 0:5) compared with u_{rms} plot from low dimensional model for the same set of modes as POD.

CONCLUSION

We have modeled the rolling mode in the wall region of a fully developed channel flow, by means of a low dimensional model. The behavior of the resulting model equations include periodic and quasi-periodic motions. The key to a rapid convergence of POD modes is the integration domain size. Since there is a justified recurrence of eddy pairs in cross-stream direction, we minimized the flow domain to contain a single eddy pair. Kinetic energy changed drastically. This study shows that, rolling mode has a dominating contributions to various turbulence statistical profiles near the walls. POD analysis shows that, stream-wise modes ($0, \pm 1$ and ± 2), POD modes (1 and 2), and cross-stream modes ($0, \pm 1, \pm 2, \pm 3, \pm 4, \pm 5$) of integration domain 2, $D2$, reconstruct u_{rms} favorably. This analysis open the door for further investigation of dynamical equations using this set of modes. The dynamical equations coefficients L, Q, and C are function of POD basis, these basis depend on the flow domain and geometry from which they are extracted. This property of POD basis limits the capability of this method to model flow with different Re and geometry and it is the only condition one should care about when applying this method as a feed back tool for control of flow or heat transfer.

ACKNOWLEDGEMENT

Financial support by the Japanese Ministry of Education, Culture, Sports, Science and Technology (MEXT) is highly acknowledged.

REFERENCES

1. Aubry, N., Holmes, P., Lumley, J. L. and Stone, E. 1988 The dynamics of coherent structures in the wall region of the turbulent boundary layer. J. Fluid Mech. 192, 115 - 173.

2. Sanghi, S. and Aubry, N. 1993 Mode interaction models for near-wall turbulence. J. Fluid Mech. 247, 455-488.

3. Berkooz, G., Holmes, P. and Lumley, J. L. 1991 Intermittent dynamics in simple models of the wall layer. J. Fluid Mech. 230, 75 - 95.

4. Berkooz, G., Holmes, P. and Lumley, J. L. 1993 The proper orthogonal decomposition in the analysis of turbulent flows. Annu. Rev. Fluid Mech. 25, 539-575.

5. Juttijudata, V., Lumley, J. L. and Rempfer D. 2005 Proper orthogonal decomposition in Squire's coordinate system for dynamical models of channel turbulence. J. Fluid Mech. 534, 195 - 225.

6. Zhou, X. and Sirovich, L. 1992 Coherence and chaos in a model of turbulent boundary layer. Phys. Fluids A 4(12), 2855 - 2874

7. Webber, G. A., Handler, R. A. and Sirovich, L. 1997 The Karhunen - Loéve decomposition of minimal channel flow. Phys. Fluids 9 (4), 1054 - 1066

8. Omurtag, A. and Sirovich, L. 1999 On Low - Dimensional modeling of Channel Turbulence. Theoret. Comput. Fluid Dynamics 13:115 - 127

9. Holmes, P., Lumley, J. L. and Berkooz, G. 1996 Turbulence, Coherent Structures, Dynamical Systems and Symmetry. Cambridge University Press.

10. Johansson, P. S., Andersson, H. I. and Rønquist E. M. 2006 Reduced - basis modeling of turbulent plane channel flow. Computers and Fluids 35: 189 - 207

11. Noack B. R., Papas, P. and Monkewitz, P. 2005 The need for a pressure - term representation in empirical Galerkin models of incompressible shear flows. J. Fluid Mech. 523, 339 - 365

12. Prabhu, R. D., Collis, S. S. and Chang, Y. 2001 The influence of control on proper orthogonal decomposition of wall-bounded turbulent flows. Phys. Fluids 13(2), 520 - 537.

13. Sirovich, L. 1987 Turbulence and the dynamics of coherent structures, parts I-III. Q. Appl. Maths XLV (3), 561 - 590.

14. Smith, T. R., Moehlis, J. and Holmes, P. 2005 Low-dimensional models for turbulent plane Couette flow in a minimal flow unit. J. Fluid Mech. 538, 71 - 110.